

Complete and incomplete fusion in the $^{28}\text{Si}+^{12}\text{C}$, ^{13}C reactions around 5 MeV/nucleon

N. Arena, Seb. Cavallaro, S. Femino', P. Figuera, S. Pirrone, G. Politi, F. Porto, S. Romano, and S. Sambataro

Dipartimento di Fisica, Università di Catania, Università di Messina, Istituto Nazionale di Fisica Nucleare,

Sezione di Catania and Laboratorio Nazionale del Sud, I-95129 Catania, Italy

(Received 28 October 1993; revised manuscript received 12 April 1994)

Velocity spectra, angular, and mass distributions of the evaporation residues produced in the reaction $^{28}\text{Si}+^{12}\text{C}$ at $E(^{28}\text{Si})=104, 115, \text{ and } 154$ MeV have been measured in the angular range $2.5^\circ \leq \vartheta_L \leq 14^\circ$. The results show for all the studied bombarding energies the presence of small contributions of incomplete fusion reactions. These small incomplete fusion components present in the evaporation-residue cross sections appear to be due to a cluster transfer reaction mechanism. Similar results have been obtained bombarding a ^{13}C target. The obtained results are compared with earlier measurements and the predictions of some existing models.

PACS number(s): 25.70.Jj

I. INTRODUCTION

The fusion reaction $^{28}\text{Si}+^{12}\text{C}$ has been extensively studied at energies above the Coulomb barrier [1–9]. Particularly, many experimental data [1–6] are available in the literature at bombarding energies not far from the Coulomb barrier, in the so-called [10] first region of the fusion excitation function, where the fusion cross section is nearly equal to the total-reaction cross section. At higher energies (second and third regions of the excitation function) the experimental data are less numerous [6–9] and the exact determination of the fusion cross sections is complicated due to the presence of other competing processes such as incomplete fusion reactions. In fact, the fraction of incomplete fusion for systems with different mass asymmetry can be correlated [11] to the center-of-mass velocity at contact of the lighter reaction partner and an onset value $v_L = (0.06 \pm 0.02)c$ (where c represents the velocity of light) has been suggested.

In this paper we report on a study of the fusion reaction $^{28}\text{Si}+^{12}\text{C}$ in the energy range 3.7–5.5 MeV/nucleon. At these energies, the corresponding v_L values vary from $0.046c$ to $0.063c$, so one can expect the presence of incomplete fusion components in the evaporation-residue cross section. We note that, in a recent study [9] of the fusion reaction $^{28}\text{Si}+^{12}\text{C}$ at bombarding energies $E(^{28}\text{Si})$ varying between 60 and 425 MeV, incomplete fusion processes have been found at the highest measured energies. At the lower energies, the authors assume that the complete fusion cross section is equal to the evaporation residue cross section. Indeed, according to the systematics of Morgenstern *et al.* [11], at bombarding energies around 170 MeV the cross sections may include as much as 10% incomplete fusion so that quite smaller incomplete fusion contributions are expected in the present work. Moreover, we remember that in our previous study [12] of the fusion reaction $^{32}\text{S}+^{12}\text{C}$ at a bombarding energy $E(^{32}\text{S})=4.5$ MeV/nucleon, we also found evidence for small incomplete-fusion contributions in the evaporation-residue cross section.

The purpose of the present work is to increase the num-

ber of experimental data available in the second region of the excitation function, to estimate the incomplete fusion cross sections at these low bombarding energies, and to identify the reaction mechanism, (e.g., cluster transfer [13] or breakup fusion [14,15]) responsible for these incomplete-fusion components. Moreover, we have bombarded a ^{13}C target with ^{28}Si at 156 MeV to investigate possible structure effects in the incomplete-fusion cross section.

The experimental procedures are described in Sec. II. The experimental results and the analysis of the velocity spectra are presented in Sec. III. The comparison of the experimental data with theoretical models and discussion are presented in Sec. IV. Finally, the conclusions are summarized in Sec. V.

II. EXPERIMENTAL PROCEDURE

The experiments were performed at the SMP Tandem accelerator facility of the Laboratorio Nazionale del Sud (LNS) in Catania. Self-supporting thin ($40 \mu/\text{cm}^2$) targets of ^{12}C were bombarded with ^{28}Si ions at 104, 115, and 154 MeV. The self-supporting target ($50 \mu/\text{cm}^2$) of ^{13}C was bombarded with ^{28}Si ions at 156 MeV. The targets were placed perpendicular to the beam direction.

The heavy ions were detected and identified by using the Gas Detector System described in detail in Ref. [16]. Briefly, the Z identification was obtained by stopping the ions in a $\Delta E - E$ ionization chamber. The mass identification was obtained by using the energy deposited in the ionization chamber and the time of flight measured between a micro-channel plate (MCP) placed at the exit of the scattering chamber and a parallel-plate avalanche counter (PPAC) in front of the ionization chamber. The flight path was 118 cm. Typical examples of charge and mass resolution are shown in Figs. 1 and 2, respectively.

Two silicon surface-barrier detectors, placed at $\pm 9^\circ$ with respect to the beam axis, were used to monitor the elastic scattering during the experiment in order to ob-

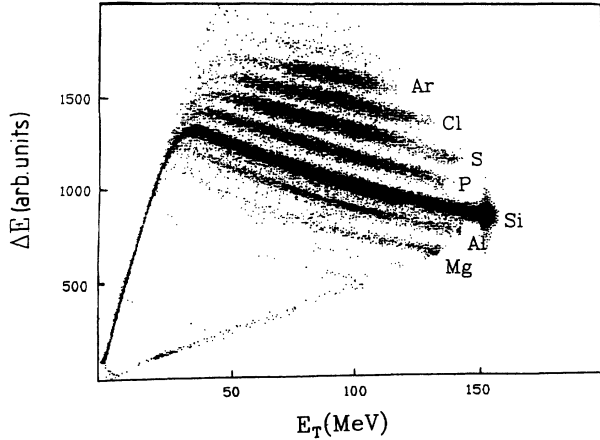


FIG. 1. Scatter plot of ΔE vs energy for the reaction $^{28}\text{Si}+^{12}\text{C}$ at 154 MeV bombarding energy and a laboratory angle of 5° .

tain the relative normalization of the measured differential cross sections. The absolute normalization constant was obtained normalizing to 1 the ratio $\sigma_{el}/\sigma_{Ruth}$ at the very forward angles.

III. EXPERIMENTAL RESULTS AND ANALYSIS

A. Elastic scattering and total-reaction cross section

The elastic scattering for the $^{28}\text{Si}+^{12}\text{C}$ system was measured over the angular range $2.5^\circ \leq \vartheta_L \leq 14^\circ$ in steps ranging from 0.5° at small angles to 2° at the larger ones.

The optical-models fits to the measured elastic-scattering angular distributions were obtained by using the code PTOLEMY [17], and are shown in Fig. 3. The experimental data at 148 MeV have been obtained in our previous elastic-scattering measurement [18]. The fit

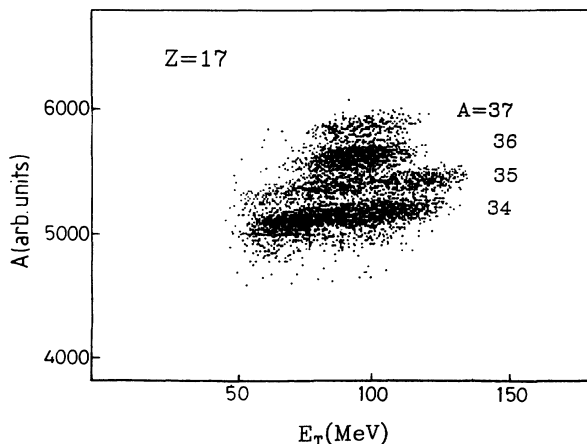


FIG. 2. Scatter plot of mass vs energy for evaporation residues with $Z=17$ at 154 MeV bombarding energy and a laboratory angle of 5° .

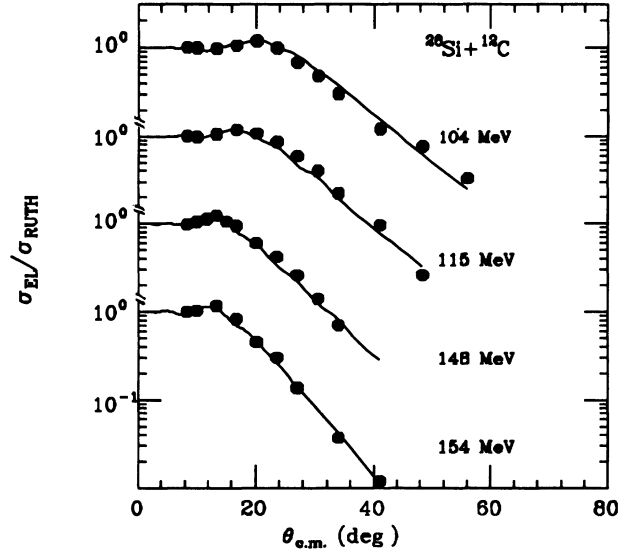


FIG. 3. Elastic-scattering cross section normalized to Rutherford scattering at various energies. The solid lines are the results of fits to the data calculated by using the code PTOLEMY.

parameters obtained are given in Table I.

In the same table the values of the total-reaction cross section $\sigma_r(\text{OM})$ obtained by means of the optical-model analysis are compared with those $\sigma_r(\text{MSOD})$ obtained by using the modified sum of differences method (MSOD) [19–21]. The two values of the total-reaction cross section are in good agreement within experimental error.

B. Analysis of the velocity spectra and incomplete fusion

Representative inclusive invariant-velocity spectra of separated individual masses for the target ^{12}C at $E(^{28}\text{Si})=154$ MeV are shown in Fig. 4. We note that the main contributions, with typical structures due to nucleon and α -particle plus nucleon evaporation, are due to evaporation residues following complete fusion.

Assuming isotropic angular distributions and Maxwellian velocity distributions for the evaporation residues recoiling in the CM, when the observed velocity distribution of the heavy residues is a symmetric Gaussian, we can conclude that these residues are formed purely by nucleon emission (xp, yn) [22,24]. In these cases, the measured invariant-velocity spectra have been fitted with the following formula obtained [24] considering the two above-mentioned assumptions:

$$\frac{1}{V_R^2} \frac{d^2\sigma}{d\Omega_L dV_R} = k \exp\left(-\frac{V_{CN}^2 \sin^2 \vartheta_L}{2s^2}\right) \times \exp\left(-\frac{(V_R - V_{CN} \cos \vartheta_L)^2}{2s^2}\right). \quad (1)$$

Here $V_{CN} \cos \vartheta_L$ is the Gaussian centroid, s is the stan-

TABLE I. Elastic-scattering optical-model fit parameters and reaction cross sections calculated from the fit [$\sigma_r(\text{OM})$] and with the MSOD method [$\sigma_r(\text{MSOD})$]. Only the well depths V_R and V_I were allowed to vary during the fit.

E_{LAB} (MeV)	V_R (MeV)	V_I (MeV)	r_{OR} (fm)	r_{OI} (fm)	a_R (fm)	a_I (fm)	σ_r (OM) (mb)	σ_r (MSOD) (mb)
104	20.0	7.61	1.30	1.30	0.55	0.55	1298	1220±120
115	15.0	9.50	1.30	1.30	0.55	0.55	1358	1280±120
148	8.00	18.0	1.30	1.20	0.55	0.55	1391	1420±100
154	11.5	20.3	1.30	1.20	0.55	0.55	1446	1430±70

standard deviation, V_R and ϑ_L are the laboratory velocity and the detection angle of the heavy residue, respectively, and k is a normalization constant. If α emission and α mixed with nucleon emission ($xp, yn, z\alpha$) compete with (xp, yn) decay channels, the complexity of the velocity spectra increases. Particularly, the velocity spectrum of a residue originated from one α and N nucleon's evaporation shows a characteristic double peak [23,24] due to the α -particle emission in the forward and backward directions. The centroids of these two peaks are shifted away from $V_{\text{CN}} \cos \vartheta_L$ by the average recoil given to the residue by the emitted α particle. To include the evaporation of the α particle in the fitting procedure, as previously pointed out in the literature [23,24], we simply replaced in the exponent of Eq. 1 $[(V_R - V_{\text{CN}} \cos \vartheta_L)^2 - V_{\text{CN}}^2 \sin^2 \vartheta_L]$ by

$$\{[(V_R - V_{\text{CN}} \cos \vartheta_L)^2 + V_{\text{CN}}^2 \sin^2 \vartheta_L]^{1/2} - V_{\alpha}\}^2 \quad (2)$$

Here V_{α} is related to the average kinetic energy re-

moved by an alpha particle. When two α particles are evaporated, the spectra show three peaks due to the possible combinations of the α -particle directions: forward-forward, forward-backward, and backward-backward. Experimental velocity distributions of single-residue masses originating from ($xp, yn, z\alpha$) have been reproduced in Eqs. (1) and (2).

In Fig. 5 are reported for each evaporation residue, at the different measured energies, the ratios of the velocity centroids $V_{\text{CN}} \cos \vartheta_L$, expected in the case of complete fusion, to the \bar{V}_R ones obtained by fitting the experimental velocity spectra using the above-mentioned formulas. As one can see, this ratio is equal to one, within the error, for all the evaporation residues. The error bars include the effect of the statistics in the fitting process and the uncertainties in the calibration procedure.

Figure 6 shows the ratios of the standard deviation s of the velocity distributions, obtained by means of the fit procedure, to the one expected in the case of complete fusion s_{CF} [23,24]:

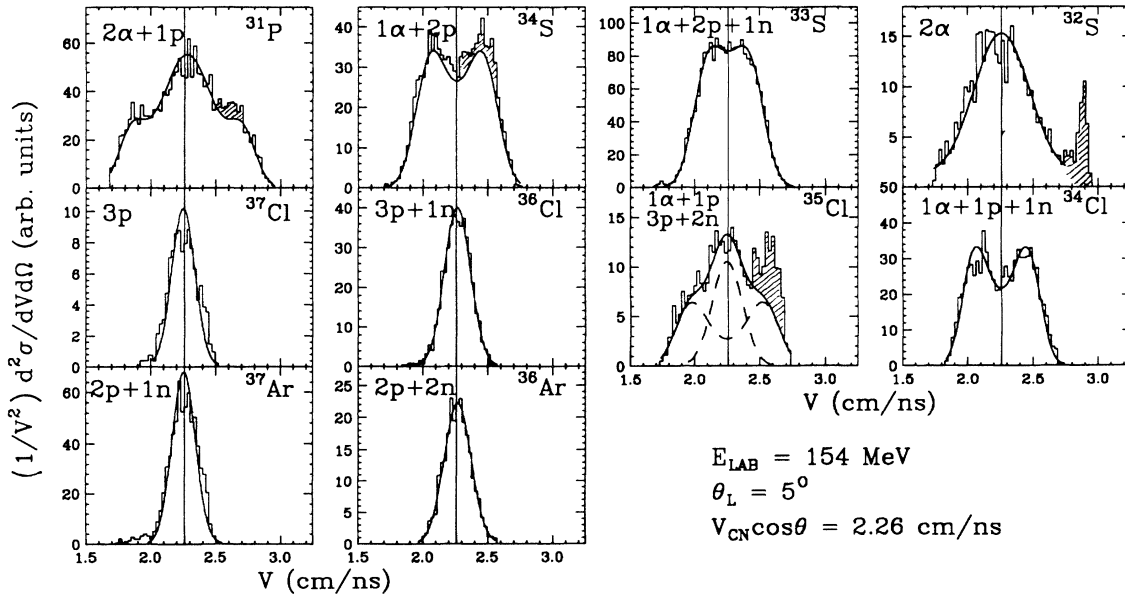


FIG. 4. Velocity spectra of evaporation residues from the reaction $^{28}\text{Si}+^{12}\text{C}$ at $\vartheta_L = 5^\circ$ and $E(^{28}\text{Si})=154$ MeV. The histograms are the experimental data, while all the curves represent the results of the fits performed as explained in Sec. III B. The vertical lines indicate the centroids expected in the case of complete fusion $V_{\text{CN}} \cos \vartheta_L$. The hatched areas originate from incomplete-fusion processes. For each residue, the number of evaporated α particles, protons (p), and neutrons (n) is indicated. In the case of ^{35}Cl , the continuous curve is obtained by summing the two dashed curves corresponding to the kinematic formulas reported in Sec. III B and representing the two different decay modes indicated in the figure ($1\alpha + 1p$ and $3p + 2n$).

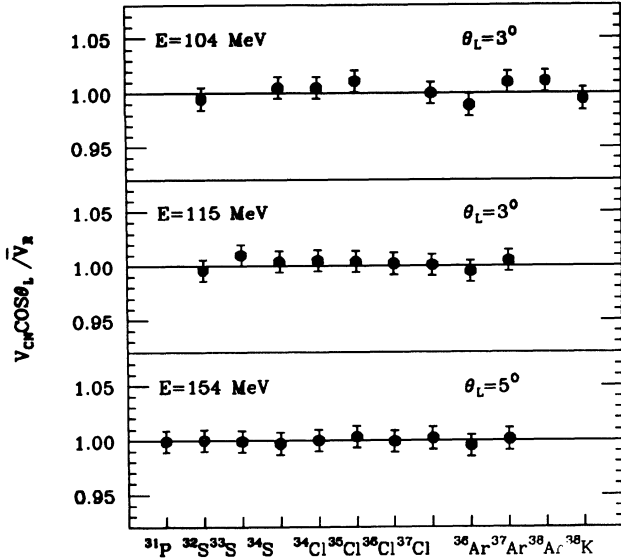


FIG. 5. Ratio of the velocity centroids expected in the case of complete fusion to those obtained by fitting the experimental velocity spectra, and plotted for the different evaporation residues.

$$s_{\text{CF}}^2 = \frac{n_{\text{evap}}}{(A_{\text{ER}})^2} T.$$

Here $n_{\text{evap}} = A_{\text{CN}} - A_{\text{ER}}$ is the number of evaporated nucleons and T is the compound-nucleus temperature, computed $T = [9.5E_{\text{exc}}/A_{\text{CN}}]^{1/2}$, where the value $A_{\text{CN}}/9.5$ for the level-density parameter is assumed. Also, in this case the experimentally extracted

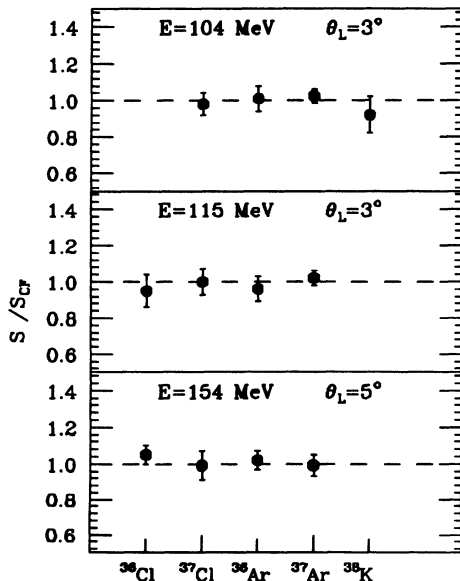


FIG. 6. Ratio of measured standard deviations (s) obtained by fitting the velocity spectra of residues produced with nucleon evaporation to the values expected in the case of complete fusion (s_{CF}).

values of s appear to be in agreement with the theoretical expectations, within the errors.

For some masses ($A = 31, 32, 34, 35$) we observe other remaining structures (hatched areas in Fig. 4), which cannot be explained as due to complete fusion. The velocities corresponding to these structures are larger than the velocity centroid $V_{\text{CN}} \cos \vartheta_L$ expected in the case of complete fusion so that, since we studied the system using reverse kinematic, we expect these structures originating from incomplete fusion [11].

Particularly, we have interpreted the hatched areas as a cross section due to incomplete-fusion reactions governed by a cluster-transfer reaction mechanism: the ^{35}Cl mass originating from ^8Be transfer ($^{28}\text{Si}+^{12}\text{C} \rightarrow ^{36}\text{Ar}^* + \alpha$; $^{36}\text{Ar}^* \rightarrow ^{35}\text{Cl} + p$) and the ^{32}S mass from α transfer ($^{28}\text{Si}+^{12}\text{C} \rightarrow ^{32}\text{S}^* + ^8\text{Be}$). Also, for the ^{34}S and ^{31}P masses the small contributions of incomplete fusion could be caused by ^8Be transfer followed by two protons and $1\alpha + 1p$ evaporation, respectively.

We draw these conclusions by comparing the implications derived from simple reaction models proposed for incomplete fusion, i.e., breakup fusion (BUF) and cluster transfer.

In fact, assuming a BUF mechanism, the ^{12}C must break into an α particle and a ^8Be in the first stage of the reaction and, successively, one of these fragments fuses with the projectile while the other fragment continues to move with almost the same velocity in the c.m. system. Following the previous description, the incomplete fusion contributions present in the ^{35}Cl and ^{32}S spectra, for example, should originate from the fusion of the projectile ^{28}Si with a ^8Be or an α particle, respectively. In this frame, at an incident energy of 154 MeV, the excitation energies of the created compound nuclei should be $E^*(^{36}\text{Ar})=40.5$ MeV and $E^*(^{32}\text{S})=18.9$ MeV. Moreover, these compound nuclei should have recoil velocities $\tilde{v}(^{32}\text{S})=2.85$ cm/ns and $\tilde{v}(^{36}\text{Ar})=2.53$ cm/ns, and possible evaporation products should be centered around a velocity equal to $\tilde{v}_{\text{CN}} \cos \vartheta_L$. As we are going to show, these calculated values imply some contradictions with the experimental results.

In fact, in the first case ($^{28}\text{Si}+^8\text{Be} \rightarrow ^{36}\text{Ar}^*$) one of the most probable decay modes for $^{36}\text{Ar}^*$ should be a single-proton evaporation, but that is unacceptable with an excitation energy of about 40 MeV. We note that, in this mass region, the mean excitation energy removed by a nucleon or an α -particle evaporation is about 16.4 MeV and 22.1 MeV, respectively [23]. In the second case ($^{28}\text{Si}+\alpha \rightarrow ^{32}\text{S}^*$) the calculated excitation energy is enough for a single-nucleon evaporation, but this evaporation is not observed experimentally.

Moreover, the experimental velocity values are incompatible with those calculated, as one can see by looking at Fig. 7. In this figure we report for ^{35}Cl and ^{32}S the ratios between the experimental velocity values of the incomplete fusion component and those calculated assuming a breakup fusion (open rhombi) or a cluster-transfer (black points) mechanism, respectively, at various angles and at 154 MeV bombarding energy. For both masses, the experimental values are larger than those calculated in the BUF frame at small angles and they are smaller at larger

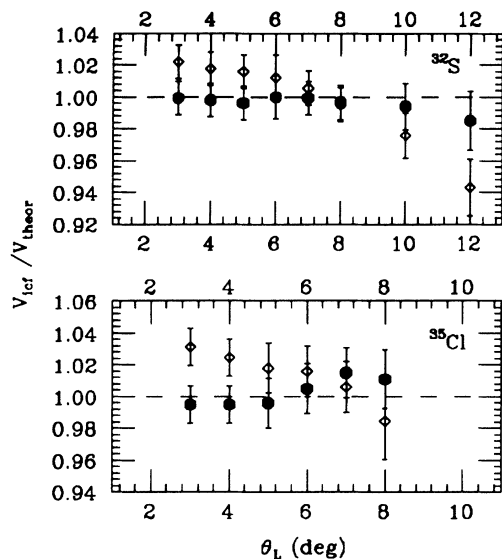


FIG. 7. Ratio of the experimental velocities of the incomplete-fusion contributions to those expected in the case of breakup fusion (open rhombs) and cluster transfer (closed circles), plotted vs laboratory angle, at $E=154$ MeV.

angles.

On the contrary, we obtain a satisfactory agreement when we interpret the observed incomplete-fusion components as products following cluster-transfer reactions. In this picture the reactions are characterized by a “ Q -value window” centered at a so-called “ Q -optimum.” Following Refs. [25,26], we can estimate a Q -optimum value, $Q_{\text{opt}} = (Z_3 Z_4 / Z_1 Z_2 - 1) E_i^{\text{c.m.}}$ [where the indices 1, 2 and 3, 4 indicate the entrance (i) and exit channel, respectively] and a corresponding excitation energy

$E^* = Q_{\text{gg}} - Q_{\text{opt}}$, where Q_{gg} is the ground-state Q value of the reaction. By using the previous formulas, we found the excitation energies $E^*(^{36}\text{Ar}) \cong 32$ MeV and $E^*(^{32}\text{S}) \cong 11$ MeV. These calculated values are in satisfactory agreement with those [$E^*(^{36}\text{Ar})=27$ MeV and $E^*(^{32}\text{S})=11$ MeV] which in two-body kinematics calculations reproduce, within the experimental error (see full points of Fig. 7) the experimental velocity values.

The excitation energy $E^*(^{32}\text{S})=11$ MeV does not allow nucleon evaporation, so it is possible to detect the ^{32}S nuclide produced in the reaction [$^{28}\text{Si}+^{12}\text{C} \rightarrow ^{32}\text{S}^* + ^8\text{Be}$]. The excitation energy $E^*(^{36}\text{Ar})=27$ MeV is consistent with a decay mode involving the evaporation of one or two nucleons in the reactions ($^{36}\text{Ar}^* \rightarrow ^{35}\text{Cl}+p$, $^{36}\text{Ar}^* \rightarrow ^{34}\text{S}+2p$). This result is in satisfactory agreement with a calculation performed with the code CASCADE [27], which predicts also the possibility of an $1\alpha + 1p$ decay. That could explain the asymmetry observed in the ^{31}P velocity spectrum. The observed preference of the proton emission in the $^{36}\text{Ar}^*$ decay could be imputed to the differences between the binding energies of the last proton and the last neutron in the considered nuclide.

Following the previous considerations, we obtained similar results for all the studies bombarding energies.

In Fig. 8 we show the invariant-velocity spectra of the evaporation residues produced in the reaction $^{28}\text{Si}+^{13}\text{C}$ at 156 MeV bombarding energy, which can be compared with those of the reaction $^{28}\text{Si}+^{12}\text{C}$ at 154 MeV. We do not observe significant differences in the evaporation residue spectra. With both targets, similar structures with comparable intensities are measured for $\gamma\alpha + xN$ evaporation following complete and incomplete fusion. The only difference in the velocity spectra of the complete fusion evaporation residues is imputable to the higher ex-

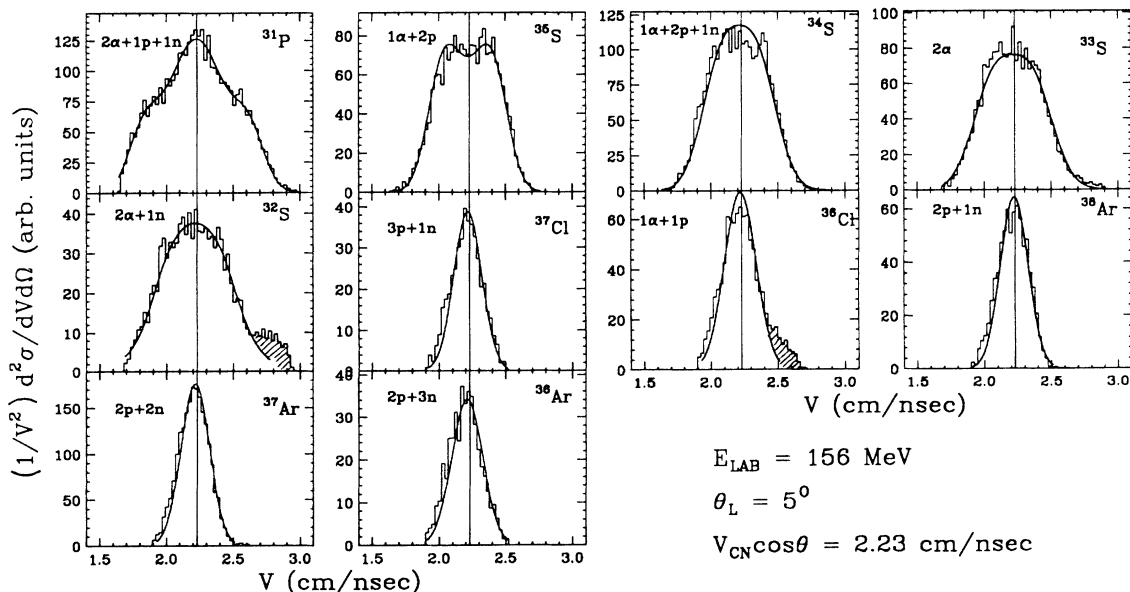


FIG. 8. Velocity spectra of evaporation residues at $\vartheta_L = 5^\circ$ of $^{28}\text{Si} + ^{13}\text{C}$ at $E=156$ MeV. The vertical lines indicate the centroid expected in case of complete fusion $V_{\text{CN}} \cos \vartheta_L$ for this reaction. The hatched areas originate from incomplete-fusion processes. For each residue, the number of evaporated α particles, protons (p), and neutrons (n) is indicated.

citation energy that in the case of the ^{13}C target favors the nucleon emission with respect to the alphas (compare the velocity spectrum of ^{35}Cl from the $^{28}\text{Si}+^{13}\text{C}$ reaction with that of ^{36}Cl from $^{28}\text{Si}+^{13}\text{C}$).

Also in this case, similar to the case of the ^{12}C target, we have interpreted the hatched areas in Fig. 8 as due to incomplete-fusion reactions originating from cluster-transfer processes with a ^4He or a ^8Be in the exit channel (i.e., ^9Be or ^5He transfer, respectively). Possible incomplete fusion events due to an ^5He transfer are not evident in the spectrum of ^{33}S . Nevertheless, as previously observed in the $^{40}\text{Ar}+^{13}\text{C}$ reaction at 7 MeV/nucleon [13], this fact could be explained by the higher excitation energy, as compared to the ^{12}C target, for the corresponding transfer reaction. In fact, at the estimated excitation energy of ^{33}S , the evaporation of a neutron is possible, and that can also explain the presence of the small, broad contribution in the ^{32}S spectrum.

C. Angular distributions

Figure 9 shows the differential angular distributions $d\sigma/d\Omega$ of the residues formed by complete and incomplete fusion as well, for the $^{28}\text{Si}+^{12}\text{C}$ reaction at 154 MeV. In the upper part of the figure it is easy to recognize the typical bell-shaped distributions of complete fusion products centered at $\vartheta_L = 0^\circ$. In the lower part the dif-

ferential angular distributions of incomplete-fusion products (the points are restricted to those angles where the subtraction of the incomplete fusion component has been possible) appear to have a very different shape, which indicates a reaction mechanism different from "breakup fusion" since, assuming this mechanism, the angular distributions should be fusionlike. Thus the hypothesis that the incomplete fusion components originate from cluster-transfer reaction, previously suggested by kinematical arguments and by excitation energy calculations, is further confirmed.

The obtained angular distributions $d\sigma/d\vartheta$ for evaporation residues following complete fusion show the typical broadening with decreasing mass due to the emission of more light particles. Integrating these angular distributions, the fusion cross sections for each evaporation residue were determined. The uncertainty in the obtained cross sections arises mainly from the normalization procedure of the data. Other small sources of error are due to the statistics of the experimental data and the uncertainty in the extrapolation of the angular distributions to small and large angles. In the same way, by integrating the angular distributions, we obtain the absolute cross sections of the evaporation residues produced in incomplete fusion reactions. The uncertainty of these latter cross sections is mainly due to the subtraction procedure of the incomplete fusion components and to the extrapolation of the angular distributions. Partial and total cross

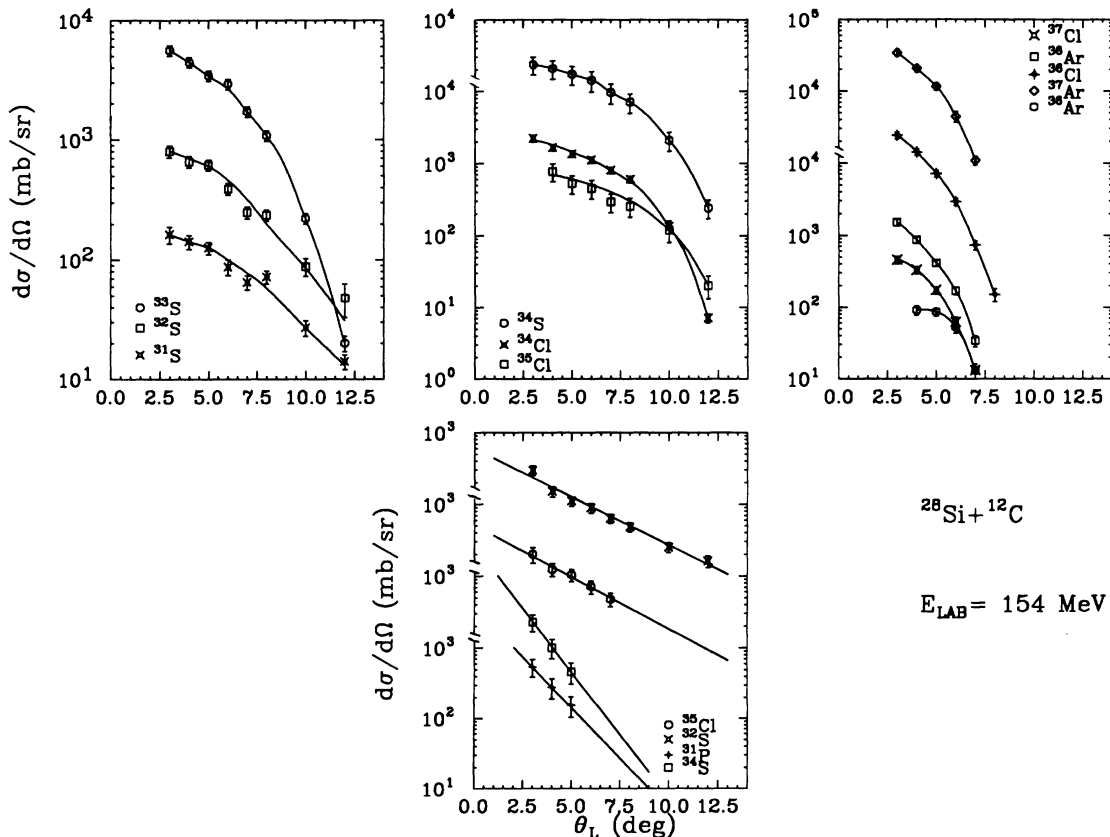


FIG. 9. Angular distributions $d\sigma/d\Omega$ of the residues from complete-fusion (top) and incomplete-fusion (bottom) reactions. The solid lines are drawn only to guide the eye.

TABLE II. Values of complete- (σ_{CF}) and incomplete- (σ_{ICF}) fusion cross sections for each evaporation residue at the three studied energies. The reported value for ^{28}Si (a) represents the cross section predicted by the evaporation code CASCADE for this residue. In the last line we report the total-fusion cross section obtained considering the measured and calculated cross sections.

	$E = 104 \text{ MeV}$		$E = 115 \text{ MeV}$		$E = 154 \text{ MeV}$	
	$\sigma_{CF} \text{ (mb)}$	$\sigma_{ICF} \text{ (mb)}$	$\sigma_{CF} \text{ (mb)}$	$\sigma_{ICF} \text{ (mb)}$	$\sigma_{CF} \text{ (mb)}$	$\sigma_{ICF} \text{ (mb)}$
^{30}Si					68±8	
^{30}P					41±5	
^{31}P	117±12		189±19		232±45	17±7
^{32}P					4±0.7	
^{33}P					3±0.6	
^{31}S					10±1.3	
^{32}S	129±14	17±7	110±13	10±4	41±5	12±5
^{33}S	14±1.7		30±3		217±22	
^{34}S	139±15		166±18		104±20	8±3
^{33}Cl					6±0.8	
^{34}Cl	48±5		81±9		89±10	
^{35}Cl	225±45	(33±13)	185±37	(26±10)	48±9	6±2
^{36}Cl	8±1		10±1.2		53±6	
^{37}Cl	12±1.7		13±1.6		11±1.3	
^{35}Ar	8±1		6±0.8			
^{36}Ar	20±2.5		15±2		32±4	
^{37}Ar	191±21		185±20		73±8	
^{38}Ar	80±10		48±5		4±0.6	
^{38}K	37±4		22±2			
$\sum \sigma$	1028±123	50±20	1060±127	36±15	1034±124	43±17
$^{28}\text{Si}^a$	30		70		80	
$\sum \sigma + \sigma(^{28}\text{Si})$	1058±123		1130±127		1114±124	

sections for complete and incomplete fusion are listed in Table II. We notice that the possible contribution of the evaporation residue ^{28}Si to the complete-fusion cross section has not been experimentally determined because of the intense background present in the ^{28}Si spectra. The values predicted by CASCADE for the cross section of ^{28}Si are 30, 70, and 80 mb at $E(^{28}\text{Si})=104, 115,$ and 154 MeV , respectively. We also have to notice that, at $E(^{28}\text{Si})=104$ and 115 MeV , the subtraction of the small incomplete fusion component in the ^{35}Cl spectra has been possible only at the two small measured angles, and the corresponding cross sections (reported between brackets in Table II) have been estimated by supposing a trend of the angular distributions similar to that obtained at $E(^{28}\text{Si})=154 \text{ MeV}$. This procedure leads to a very large error in the incomplete fusion component which can explain the decreasing cross section with increasing incident energy, in contrast to theoretical expectations.

IV. COMPARISON WITH THEORY AND DISCUSSION

The experimental cross sections of the different evaporation residues following complete fusion produced at 104, 115, and 154 MeV bombarding energies are shown in Fig. 10 together with the statistical-model predictions computed by using the code CASCADE [27].

We used in the input of CASCADE the complete fusion cross sections reported in Tables II and III and a diffuseness for the transmission coefficients in the entrance channel $d = 2$. A level-density parameter $a = A/9.5$ has

been used in the high excitation energy region. In general there is good agreement at all the considered energies.

For the evaporation residues formed by α evaporation, we compared the average kinetic energies of the evaporated α particles, extracted from the distance of the two peaks in the experimental velocity spectra, with those obtained by using the case CASCADE at all the studied bombarding energies. The results are in satisfactory agreement, even though the α energies predicted by CASCADE are slightly greater than the experimental ones.

In Fig. 11 we plotted most of the available fusion cross sections for the $^{28}\text{Si}+^{12}\text{C}$ system as a function for $E_{c.m.}^{-1}$. We notice that the present results, shown as full symbols, are obtained by summing the measured values of the evaporation-residue cross section following complete fusion with the cross section for ^{28}Si predicted by the code CASCADE.

As one can see, our experimental results, located in the second energy region of the fusion excitation function, link up very well with the data of Nagashima [4] and appear to be in good agreement with the results of Vineyard *et al.* [9].

In the same figure we reported the predictions of the critical-distance fusion model [28] (dot-dashed curve), the proximity fusion model [29] (solid curve), and the Bass model [30] (dashed curve).

We note that the empirical nuclear potential of Bass is specified by the function

$$V_n(s) = \frac{R_1 R_2}{R_1 + R_2} g(s) ,$$

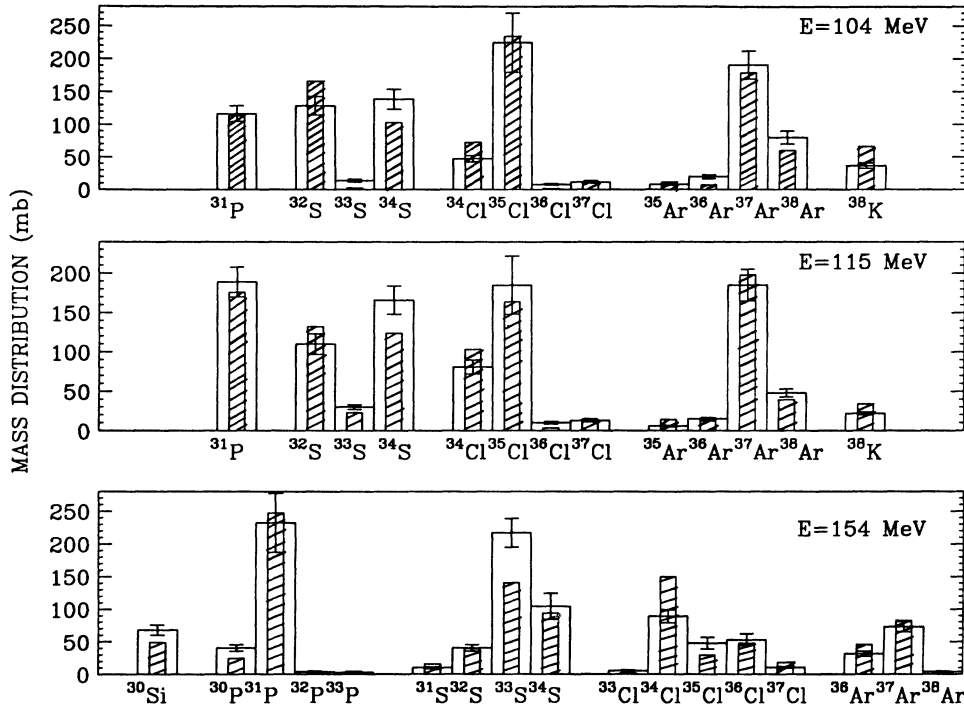


FIG. 10. Mass distributions of evaporation residues. The experimental data are plotted as open histograms, while the hatched bars are the yields predicted from the evaporation code CASCADE.

where

$$g(s) = [A \exp(s/d_1) + B \exp(s/d_2)]^{-1} .$$

The parameter values used in the calculation are those reported in Ref. 30, based on a global fit to fusion data, i.e., $A = 0.03 \text{ MeV}^{-1} \text{ fm}$, $B = 0.006 \text{ MeV}^{-1} \text{ fm}$, $d_1 = 3.30$

fm, and $d_2 = 0.65 \text{ fm}$. The choice of these parameters, rather than those used in Ref. [7], is due to the better agreement that we obtain within the theoretical curve with our experimental data and the high-energy data [9]. A much better agreement is obtained comparing our experimental points and the high-energy data [9] with the predictions of the proximity fusion model [29], which

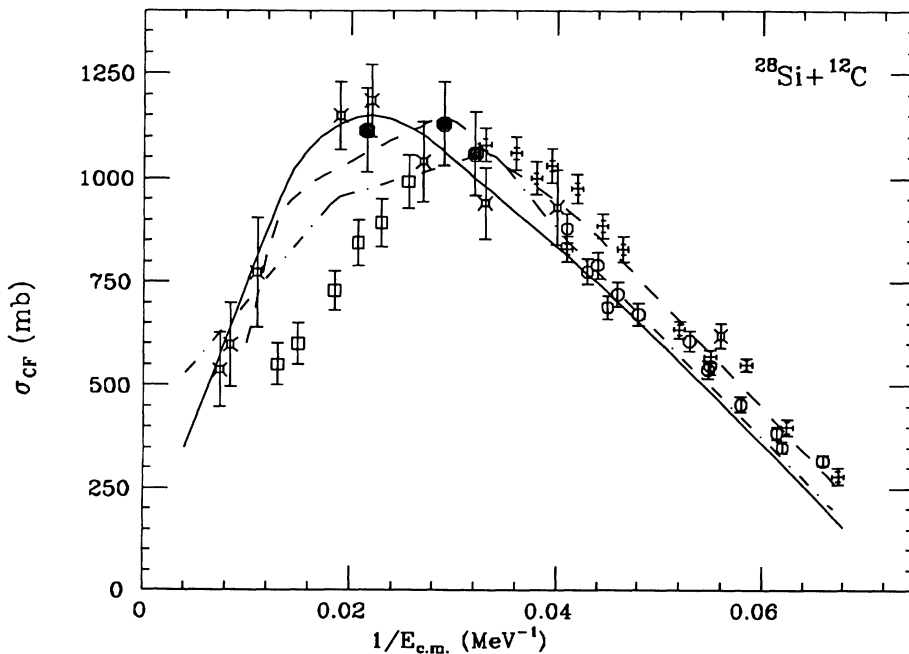


FIG. 11. Complete-fusion cross sections for the $^{28}\text{Si} + ^{12}\text{C}$ system as a function of E_{CM}^{-1} . The squares are the data reported by Harmon *et al.* [7,8], the open circles those by Gary and Volant [2], the open squares with diagonal cross those by Vineyard *et al.* [9], and the crosses those by Nagashima *et al.* [4]; all the data are quoted with the errors indicated by the same authors. The full symbols are the data of the present work. The curves represent the predictions of the critical-distance fusion model [28] (dot-dashed), the proximity fusion model [29] (solid), and the Bass model [30] (dashed).

reproduce very well the excitation function's maximum value.

The critical angular momenta l_{cr} extracted from the complete-fusion cross sections, which include the ^{28}Si yields, using three sharp cutoff approximation are reported in Table III. The uncertainty in the l_{cr} represents the experimental uncertainty in the cross section. In Fig. 12 we report the critical angular momenta for the fusion of several systems $^{28}\text{Si}+^{12}\text{C}$ [2,4,7-9], $^{20}\text{Ne}+^{20}\text{Ne}$ [31], and $^{16}\text{O}+^{24}\text{Mg}$ [32], leading to the same compound nucleus ^{40}Ca at various excitation energies; the present results are marked by arrows. The solid curve shown in the figure is the statistical yrast line [33] calculated with $r_0 = 1.2$ fm and $\Delta Q = 10$ MeV.

We see that our experimental results are reproduced rather well by this parametrization. Our point at $E(^{28}\text{Si})=154$ MeV appear to be larger than the saturation value of about $22\hbar$, extracted by Harmon *et al.* [7,8], which indicates the existence of an entrance-channel imposed limit on the high-energy fusion cross section. Because of the limited energy range we explored and the experimental uncertainties, we are not able to rule out the possibility of an entrance-channel limitation on the complete-fusion cross section. However, we observe that, as can be seen in Fig. 11, our data are in very good agreement with the Bass-model calculation [30] and the proximity fusion model [29], which leads to a critical angular momentum in the entrance channel l_{cr}^{fus} of $29\hbar$ [7].

The value is confirmed from the high-energy experimental data of Vineyard *et al.* [9], which show a saturation value of the critical angular momentum at about

TABLE III. Critical angular momenta for complete fusion and corresponding cross sections at the three measured energies. The reported cross sections include the contribution of the evaporation residue ^{28}Si predicted by the code CASCADE.

E_{LAB} (MeV)	$E_{c.m.}$ (MeV)	σ_{CF} (mb)	l_{cr} (\hbar)
104	31.5	1058 ± 123	19.6 ± 1.2
115	34.5	1130 ± 127	21.3 ± 1.3
154	46.2	1114 ± 124	24.7 ± 1.5

$29\hbar$, consistent with the value at which the fission barrier of the ^{40}Ca compound nucleus vanishes, as calculated with the Sierk model [34].

The ratios of the complete-fusion cross sections (σ_{CF}) to the total evaporation-residue cross sections ($\sigma_{\text{CF}} + \sigma_{\text{ICF}}$), extracted from the present data, appear to be in agreement with the trend established by the incomplete-fusion systematics of Morgenstern *et al.* [11], as shown in Fig. 13. In this figure the present data are reported, together with the results of other authors, for ^{28}Si -induced reactions as a function of V_L/c . The full curves represent the systematic trend extracted in Ref. [11], where it has been shown that the results for symmetric and asymmetric systems fall mainly along the lower and upper curve, respectively. We notice that, for values of V_L/c near the suggested threshold, we still find evidence for small incomplete-fusion components in the measured velocity spectra.

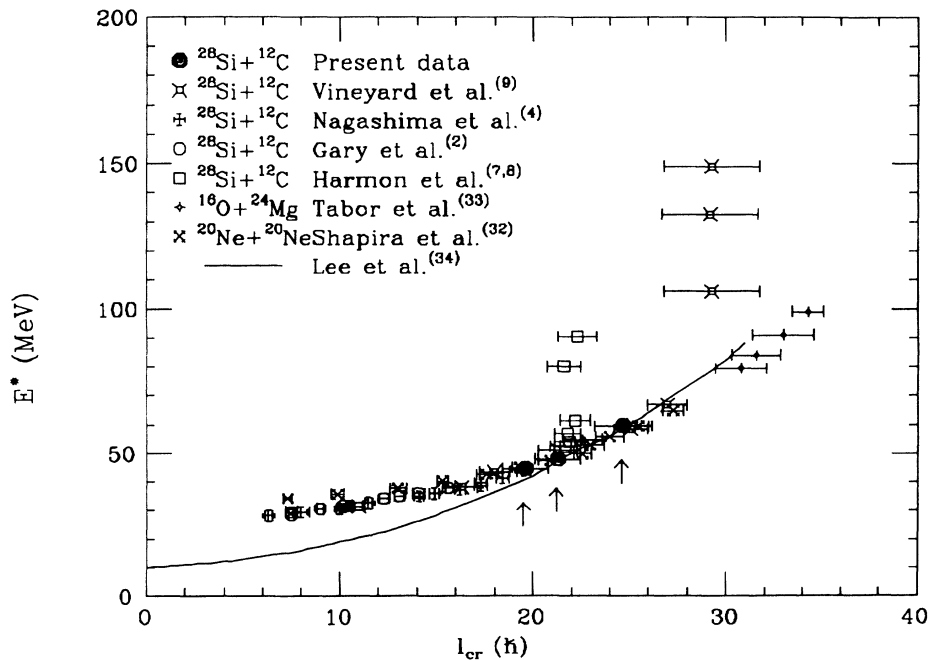


FIG. 12. Critical angular momenta for different complete-fusion reactions leading to the formation of the compound nucleus ^{40}Ca at different excitation energies; the present results are marked by arrows. The solid curve represents the statistical yrast line [33] calculated with $r_0 = 1.2$ fm and $\Delta Q = 10$ MeV.

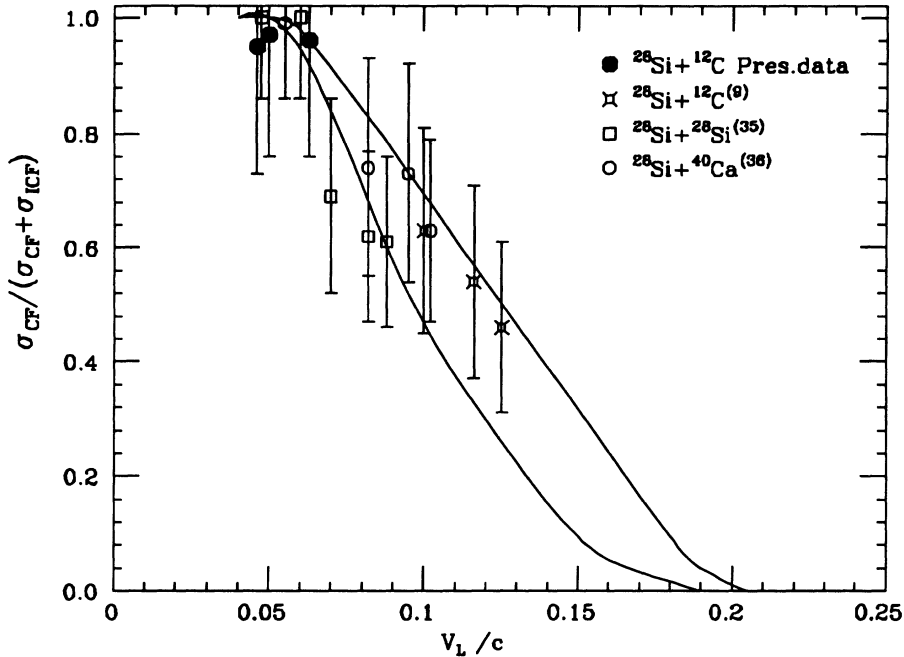


FIG. 13. Ratios of complete-fusion cross section to the total evaporation-residue cross section as a function of V_L/c , for different ^{28}Si -induced reactions. The full symbols are the present data. The curves represent the systematic trends extracted from the incomplete-fusion systematics of Ref. [11].

V. CONCLUSION

We have presented the elastic-scattering cross sections and the mass and angular distributions for the evaporation residues produced in the reaction $^{28}\text{Si}+^{12}\text{C}$ at bombarding energies ranging from 3.7 to 5.5 MeV/nucleon. The total-reaction cross sections obtained by using the modified SOD method are in good agreement with the values extracted by means of the optical-model analysis.

From the analysis of the evaporation-residue velocity spectra, we deduce that the main contributions to the evaporation-residue cross sections originate from a complete fusion mechanism, but for all studied energies incomplete fusion components are present. The kinematical analysis, the excitation energies, and the trend of the angular distributions suggest that we interpret these incomplete fusion events as reaction products generated by cluster-transfer reactions. This conclusion is in agreement with the results of Ref. [13], where it is shown that, in the mass range here considered, a “transferlike” mechanism is responsible for the incomplete fusion reactions at low bombarding energies. The values of the incomplete-fusion cross sections are in agreement with a previously

established systematic [11], which correlates the fraction of incomplete fusion with the center-of-mass velocity at contact with the lighter reaction partner and with the mass asymmetry in the entrance channel. Similar velocity spectra with incomplete fusion components are obtained by bombarding a ^{13}C target. The experimental data of the present work are in good agreement with earlier measurements of the $^{28}\text{Si}+^{12}\text{C}$ system and with theoretical predictions.

Finally, the critical angular momenta extracted from the complete-fusion cross section seem to be consistent with the fusion cross section limitation expected in the frame of the liquid-drop limit, as suggested in Ref. [9].

ACKNOWLEDGMENTS

The authors wish to thank the Laboratorio Nazionale del Sud (Catania) accelerator staff for their assistance in providing the beam used in the experiment. Thanks are due to Mr. V. Campagna and Mr. G. Poli for their technical help during the measurements.

- [1] W.J. Jordan, J.D. Maher, and J.C. Peng, *Phys. Lett.* **87B**, 38 (1979).
- [2] S. Gary and C. Volant, *Phys. Rev. C* **25**, 1877 (1982).
- [3] K.P. Lesko, D.K. Lock, A. Lazzarini, R. Vandenbosch, V. Metag, and H. Doubre, *Phys. Rev. C* **25**, 872 (1982).
- [4] Y. Nagashima, S.M. Lee, M. Sato, J. Schinizu, T. Nakagawa, Y. Fukuchi, K. Furuno, M. Yamanouchi, and T. Mikamo, *Phys. Rev. C* **26**, 2661 (1982).

- [5] M. Hugi, J. Lang, R. Muller, E. Ungricht, K. Bodek, L. Jarczyk, D. Ramys, A. Magiera, A. Strzalkowski, and G. William, *Nucl. Phys.* **A368**, 173 (1981).
- [6] Zheng Ji-wen *et al.*, in *Proceedings of the International Conference on Nuclear Physics*, Florence, 1983, edited by P. Blasi and R. A. Ricci (Tipografia Compositori, Bologna, 1983), Vol. 1, p. 545.
- [7] B.A. Harmon, S.T. Thornton, D. Shapira, J. Gomez del

- Campo, and M. Beckerman, *Phys. Rev. C* **34**, 552 (1986).
- [8] B.A. Harmon, D. Shapira, P.H. Stelson, B.L. Burks, K.A. Erb, B. Shivakumar, K. Teh, and S.T. Thornton, *Phys. Rev. C* **38**, 572 (1988).
- [9] M.F. Vineyard, J.F. Mateja, C. Beck, S.E. Atencio, L.C. Dennis, A.D. Frawley, D.J. Henderson, R.V.F. Janssens, K.V. Kemper, D.G. Kovar, C.F. Maguire, S.J. Padalino, F.W. Prosser, G.S.F. Stephans, M.A. Tiede, B.D. Wilkins, and R.A. Zingarelli, *Phys. Rev. C* **47**, 2374 (1993).
- [10] Ch. Ngo, *Prog. Part. Nucl. Phys.* **16**, 139 (1986).
- [11] H. Morgenstern, W. Bohne, W. Galster, K. Grabisch, and A. Kyanowski, *Phys. Rev. Lett.* **52**, 1104 (1984).
- [12] N. Arena, S. Cavallaro, S. Femino', P. Figuera, S. Pirrone, F. Porto, and S. Sambataro, *Phys. Rev. C* **44**, 1947 (1991).
- [13] H. Morgenstern, W. Bohne, W. Galster, and K. Grabisch, *Z. Phys. A* **324**, 443 (1986).
- [14] T. Udagawa and T. Tamura, *Phys. Rev. Lett.* **45**, 1311 (1980).
- [15] E. Takada, T. Shimoda, N. Takahashi, T. Yamaya, K. Nagatani, T. Udagawa, and T. Tamura, *Phys. Rev. C* **23**, 722 (1981).
- [16] P. Figuera, S. Pirrone, A. Anzalone, N. Arena, S. Cavallaro, S. Femino', F. Giustolisi, F. Porto, and S. Sambataro, *Il Nuovo Cimento A* **104**, 251 (1991).
- [17] M.H. Farlane and S.C. Poeper, Argonne National Laboratory Report No. ANL- 76-11 (1978).
- [18] P. Figuera, Ph.D. thesis Universita' di Catania, 1993.
- [19] R. Giordano, F. Porto, S. Sambataro, and A. Scalia, *Il Nuovo Cimento A* **61**, 182 (1981).
- [20] R. Giordano, F. Porto, S. Sambataro, and A. Scalia, *Lett. Nuovo Cimento* **31**, 189 (1981).
- [21] F. Porto and S. Sambataro, *Il Nuovo Cimento A* **83**, 339 (1984).
- [22] J. Gomez del Campo, R.G. Stokstad, J.A. Biggerstaff, R.A. Dayros, A.H. Snell, and P.H. Stelson, *Phys. Rev. C* **19**, 2170 (1979).
- [23] H. Morgenstern, W. Bohne, W. Grabisch, H. Lehr, and W. Stöffler, *Z. Phys. A* **313**, 39 (1983).
- [24] W. Galster, H. Morgenstern, W. Bohne, K. Grabisch, and A. Kyanowski, in *Proceedings of the Tsukuba International Symposium*, edited by K. Furuno and T. Kishimoto (World Scientific, Singapore 1984), p. 248.
- [25] Ch. Toepffer, *Z. Phys* **253**, 78 (1972).
- [26] P.J.A. Buttle and L.J.B. Goldfarb, *Nucl. Phys.* **A176**, 299 (1979).
- [27] F. Pühlhofer, *Nucl. Phys.* **A280**, 267 (1977).
- [28] T. Matsuse, A. Arima, and S.M. Lee, *Phys. Rev. C* **26**, 2338 (1982).
- [29] J.R. Birkelund, L.E. Tubbs, J.R. Huizenga, J.N. De, and D. Sperber, *Phys. Rep.* **56**, 107 (1979).
- [30] R. Bass, *Phys. Rev. Lett.* **39**, 265 (1977).
- [31] D. Shapira, D. Di Gregorio, J. Gomez del Campo, R.A. Dayras, J.L.C. Ford Jr., A.H. Snell, and P.H. Stelson, *Phys. Rev. C* **28**, 1148 (1983).
- [32] S.L. Tabor, D.F. Geesaman, W. Henning, D.G. Kovar, and K.E. Rehm, *Phys. Rev. C* **17**, 2136 (1978).
- [33] S.M. Lee, T. Matsuse, and A. Arima, *Phys. Rev. Lett.* **45**, 165 (1980).
- [34] A.J. Sierk, *Phys. Rev. Lett.* **55**, 582 (1985); *Phys. Rev. C* **33**, 2039 (1986).
- [35] M.F. Vineyard, J.S. Bauer, C.H. Gosdin, R.S. Trotter, D.G. Kovar, C. Beck, D.J. Henderson, R.V.F. Janssens, B.D. Wilkins, G. Rosner, P. Chowdhury, H. Ikezoe, W. Kuhn, J.J. Kolata, J.D. Hinnefeld, C.F. Maguire, J.F. Mateja, F.W. Prosser, and G.S.F. Stephans, *Phys. Rev. C* **41**, 1005 (1990).
- [36] M.F. Vineyard, J.S. Bauer, J.F. Crum, C.H. Gosdin, R.S. Trotter, D.G. Kovar, C. Beck, D.J. Henderson, R.V.F. Janssens, B.D. Wilkins, C.F. Maguire, J.F. Mateja, F.W. Prosser, and G.S.F. Stephans, *Phys. Rev. C* **45**, 1784 (1992).

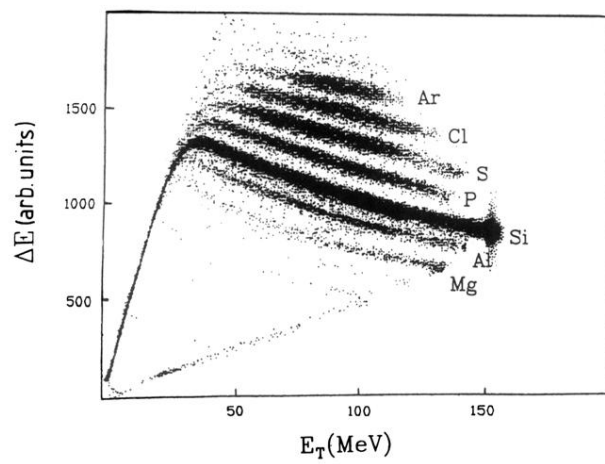


FIG. 1. Scatter plot of ΔE vs energy for the reaction $^{28}\text{Si}+^{12}\text{C}$ at 154 MeV bombarding energy and a laboratory angle of 5° .

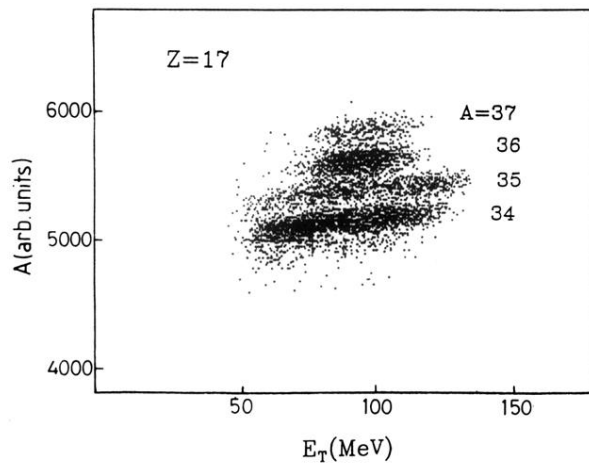


FIG. 2. Scatter plot of mass vs energy for evaporation residues with $Z=17$ at 154 MeV bombarding energy and a laboratory angle of 5° .